Structural parameter study of dual transducers-type ultrasonic levitation-based transportation system

Guanyu Mu[1], Jie Zhao[1,*], Huijuan Dong[1,**], Jiang Wu[2,***], Kenneth Thomas Victor Grattan[3], Tong Sun[3]

1. State Key Laboratory of Robotics and System, Harbin Institute of Technology, Harbin 150001, China

2. School of Control Science and Engineering, Shandong University, Jinan 250061, China.

3. School of Mathematics, Computer Science and Engineering, City University of London, London EC1V 0HB, U. K.

Corresponding authors:

* Jie Zhao: jzhao @ hit.edu.cn

** Huijuan Dong: dhj @ hit.edu.cn

*** Jiang Wu: wujiang @ sdu.edu.cn

Abstract: Having a continuous mode of transportation, in the manufacturing and pharmaceutical industries, is desirable and this facilitated by the usage of dual transducer-type ultrasonic levitation-based transportation systems. It is well known that the structural and electrical parameters determine what can be transported continuously, but the relationships between these important parameters are still not clear. In this study, the vibrating plate length and the phase shift between the two transducers were investigated as both of these are key parameters for the transportation system, and affect the standing wave ratios (SWRs), the acoustic radiation forces, and consequently the way the transportation system operates. Through numerical analysis and experimental verification, it can be seen that when the sum or difference of the spatial phase difference (determined by the vibrating plate length) and the phase shift is equal to $180°\times(1+2n)$ (where n is an integer), except for the spatial phase difference of $180°\cdot m$ (where m is also an integer) and the SWRs approaches unity, all this implying that traveling waves (TWs) are dominantly excited on the vibrating plate. As a consequence, the TW-induced acoustic radiation force, which greatly exceeds the standing wave-induced force, causes the continuous transportation of the particle being moved in the sound field. This paper not only clarifies the requirements for generating this continuous transportation, but also provides valuable information on the practical design of such a transportation system.

Keywords: Ultrasonic levitation-based transportation system, dual transducers type, acoustic force, standing wave ratio, spatial phase difference.

I. Introduction

Recently, the non-contact transportation of small objects, powders, and liquid droplets has attracted significant attention from the manufacturing and pharmaceutical industries [1–5]. Compared to air pressure- or magnetic-/electric field-levitation-based transportation, the use of ultrasonic levitation-based transportation shows relatively high cost-efficiency, operates in the absence of electromagnetic radiation, and there is no special requirement on the levitated objects used [6–9]. To date, it has been reported that ultrasonic levitation-based transportation has been achieved with the following types of instruments: (1) the Excitor-absorber systems. Here, Hashimoto *et al*. [10] had utilized two transducers, one of which acted as an exciter while the other as an absorber, to generate a traveling wave (TW) for transporting a planar object. Following this principle, Ito *et al.* [11,12] had substituted a rubber plate for one transducer, as the absorber, to simplify the configuration. In general, continuous transportation is achieved with the Excitor-absorber system, using the condition where the vibrational energy is perfectly absorbed [13] – this is, however, difficult to achieve in most cases [13]. (2) Levitating-moving systems. As a typical example, Hashimoto *et al.* [14] fixed a Langevin transducer, capable of generating a standing wave (SW) to levitate an object, onto a stage, and thus translational transportation by moving the stage was achieved. Though large objects are transportable, the distance over which this can happen is limited by the range of the stage [14]. Further, when the stage accelerates or decelerates sharply, the object will easily fall down, because the horizontal component

of the acoustic radiation force is insufficient [15]. (3) Multi-transducers systems. As an example, Foresti *et al.* [16] had arranged a series of transducers and adjusted their driving voltages to ensure the translational transportation of a particle. Ochiai and Hoshi [17–19] had adapted four ultrasonic transmitters, each of which comprised 285 transducer elements, to form a sound field which could be modulated and thus obtained the three-dimensional manipulation of several dozen small particles. These systems exhibit high controllability of the particles used, but they would be difficult to use in practical applications, because of their complicated structures.

In a way that is different from the above methods, Koyama and Nakamura [20–23] developed a dual transducer-type system to transport particles and/or droplets, using ultrasonic methods. The system has the following features: (1) The core parts contain two transducers and two plates, so a compact structure would be easy to obtain [21]. (2) Based on their structural and electrical parameters, the transportation system developed works using the continuous or step mode [20,23]; the transportation system offers a high speed in the continuous mode, while good accuracy is achieved in the step mode [20,23]. Thus, it is very important to conduct a deeper investigation into the properties of dual transducer-type ultrasonic levitation-based transportation systems.

For most types of application, e.g. automatic production lines, the transportation system needs to work in the continuous mode [23,24]. It can be predicted that the structural and electrical parameters of the system affect the generation of the continuous mode [20], but the optimum method for

determining these parameters has not, as yet, been fully studied. Considering that this is essential in the practical design of the transportation system, it is important to clarify the requirements for the vibrating plate length and the phase shift for generating the continuous mode of operation. Here, the vibrating plate length and the phase shift are discussed prior to the other parameters, because they so markedly affect the transportation performance [8]. In addition, there are generally some specific requirements for the vibrating plate length because of the space limitations in any practical system [20,21]. It should be noted that the phase shift should be adjusted based on the vibrating plate length to ensure good transportation performance.

To do so, first the dual transducer-type ultrasonic levitation-based transportation system configuration and an equivalent transducer array model, capable of describing the vibration properties, are introduced. Then, the way that the SWR and the acoustic radiation force (both of which strongly affect the working mode) relate to the vibrating plate length and the phase shift is discussed, through the usage of the numerical analysis carried out. Following that, a series of experiments has been carried out with a view to verifying the results of the simulation using the numerical techniques discussed.

II. Configuration of levitation system and equivalent transducer array model

As shown in Fig. 1, the transportation system comprises primarily of two Langevin transducers (1#

and 2#), a vibrating plate, a planar reflecting plate and a frame; these components are connected together. When two different voltages, with a phase shift between them, were applied to the two transducers through two different channels, TWs and SWs simultaneously were seen on the vibrating plate and a sound field was generated between the vibrating plate and the reflecting plate. The aluminum vibrating plate, whose length, l, was varied in this work, was comprised of two free ends and a supported portion. Here, aluminum is chosen as the vibrating plate owing to its low density and good workability. Previous studies [13] have reported that the optimal length of the free end was equal to half the wavelength of the flexural vibration.

Fig. 2 illustrates the Langevin-type longitudinal transducer, which consists of four lead-zirconate-titanate disks (PZT-8), a steel end cap (45# in the Chinese standard) and a titanate-alloy horn (TC-8). The transducer has a length of 357 mm, which equals 1.5 wavelengths. To efficiently excite the longitudinal vibration, the PZT disks were 5 mm in thickness, of 15 mm inner diameter and 35 mm outer diameter and were arranged to be at a node. The end cap, whose diameter was identical to those of the PZT disks, has a length of 36.8 mm. The horn, whose end surface has an area of 35×10 mm^2, was exponential in shape and contained several cylindrical parts, of different diameters. The cylindrical part was 5 mm in thickness and of 45 mm outer diameter and was clamped to the frame.

The transducer equivalent circuit parameters were measured to show the electrical properties of the Langevin transducer. The series frequency, f_s, the parallel frequency, f_p, the bandwidth corresponding

to 0.707 times the maximum admittance, Δf, the motional admittance, Y_m, and the clamped capacitance, C_d, were obtained using an impendence analyzer (type 4294A, Agilent). The mechanical quality factor, Q, the motional resistance, R_m, the motional induction, L_m, and the motional capacitance, C_m, were calculated as discussed in the literature [25,26]

$$Q = \frac{f_s}{\Delta f}, \tag{1}$$

$$R_m = \frac{1}{Y_m}, \tag{2}$$

$$L_m = \frac{Q}{2\pi f_s \cdot Y_m}, \tag{3}$$

and

$$C_m = \frac{2\pi f_s \cdot Q}{Y_m}, \tag{4}$$

respectively. Table I demonstrates that the electrical circuit parameters of Transducer 1# do not greatly differ from those of Transducer 2#; this contributes to exciting TWs and/or SWs as were designed [27]. In addition, their serial frequencies were ~33.4 kHz, which was treated as the working frequency when designing the transportation system.

An equivalent transducer-array model was developed by the authors, as shown in Fig. 3, to deepen the understanding of the working principles. As shown in Fig. 3(a), the vibration velocity is zero at $t = nT$ and reaches its maximum value at $t = (n + 1/4)T$, where t represents time, n is an integer and T denotes the period of the wave propagating along the vibrating plate. Taking two points A and B as examples, the vibration velocity at point A is given as

$$v_A(t) = V_0 \cos(\omega t)\cos(kx_A), \tag{5}$$

where ω and k represent the angular frequency ($\omega = 2\pi f_s$) and the wavenumber, respectively; and the vibration velocity at point B, which is located at a distance of half a wavelength ($\lambda_b/2$) from point A, can be expressed as

$$\begin{aligned} v_B(t) &= V_0 \cos(\omega t)\cos(kx_B) \\ &= V_0 \cos(\omega t)\cos\left[k\left(x_A \pm \frac{\lambda_b}{2}\right)\right] \\ &= V_0 \cos(\omega t)\cos(kx_A \pm 180°) \\ &= V_0 \cos(\omega t \mp 180°)\cos(kx_A). \end{aligned} \tag{6}$$

Eqs. 5 and 6 demonstrate that, since the vibration velocity at point B has a 180° phase difference from that of point A, the vibrating plate can be expressed in the equivalent model as an array of transducers, as shown in Fig. 3(b), where those that are adjacent vibrate at 180° out of phase from each other [see Fig. 3(c)]. This model demonstrates that the length of the supported portion must be $n\lambda_b/2$ (where n is an integer) to excite a resonant state (or a SW) on the vibrating plate, while TWs and SWs simultaneously exist where the length was $n\lambda_b/2 + \Delta l$ (where $\Delta l < \lambda_b/2$). Here, λ_b can be derived as shown in [28]

$$\lambda_b^2 = \sqrt{\frac{E}{12\rho(1-\sigma^2)}} \cdot h \cdot \frac{2\pi}{f_s}, \tag{7}$$

where E (= 72 GPa), ρ (= 2.8×10^3 kg/m^3), and σ (= 0.33) respectively denote the Young's modulus, the density, and Poisson's ratio of aluminum; and h (= 3 mm) represents the thickness of the vibrating plate. According to Eq. 7, λ_b can be calculated to be equal to 30.1 mm, at 33.4 kHz.

III. SWR and acoustic radiation force

A. SWR

Initially, the way in which the SAW thickness depends on the vibrating plate length and the phase shift can be seen, using the following approach:

(1) *Build the wave equation.* When two transducers are excited with a phase shift, θ, (as shown in Fig. 1), the wave propagating along the vibrating plate, of length, l, can be expressed as [29]:

$$v(x,t) = V_0 \cos(\omega t)\cos(kx) + V_0 \cos(\omega t + \theta)\cos\left[k(l-x)\right]. \tag{8}$$

(2) *Calculate the root mean square of Eq. 8*, as discussed in [28]

$$\begin{aligned} v_e(x) &= \sqrt{\frac{\omega}{2\pi} \cdot \int_{-\frac{\pi}{\omega}}^{\frac{\pi}{\omega}} v^2(x,t)\,dt} \\ &= V_0 \cdot \sqrt{\frac{1}{2}\cos^2(kx) + \cos(kx)\cos\left[k(l-x)\right]\cos(\theta) + \frac{1}{2}\cos^2\left[k(l-x)\right]}. \end{aligned} \tag{9}$$

(3) *Derive the SWR*, as discussed in the literature [13,28,30]

$$SWR = \frac{v_{e-\max}}{v_{e-\min}}, \tag{10}$$

where $v_{e\text{-}max}$ and $v_{e\text{-}min}$ respectively stand for the maximum and minimum amplitudes of $v_e(x)$ (see Eq. 9 for its definition), within a half wavelength of the vibrating plate.

Fig. 4 shows a plot of the variation of the SWRs against the phase shift, at l = 310 mm. Since λ_b = 30.1 mm, the spatial phase difference, φ, [defined as 360°× (l/λ_b)] between the supported portion of the two transducers is ~(10 × 360°) + 120°. As can be seen, when $\theta = \pm 60°$, the SWRs are equal to one, indicating that the TWs are excited on the vibrating plate. Fig. 5 illustrates how the SWRs

depend on the phase shift and the length of the vibrating plate. Clearly, the SWRs approach unity in the cases where

$$\begin{cases} |\theta - \varphi| = 180^\circ \cdot (1+2n) \\ |\theta + \varphi| = 180^\circ \cdot (1+2n) \end{cases}. \quad (11)$$

Note that, at l = 285, 300 and 315 mm [corresponding to φ = (10×360°)-180°, (10×360°), and (10×360°)+180°], the SWRs theoretically approach infinity, which implies that the particle is not transportable, although φ and θ satisfy the relationships given in Eq. 11.

B. Acoustic radiation force

Subsequently, Finite Element Analysis (FEA) was implemented to derive the SW-induced acoustic radiation force. Fig. 6(a) shows a simplified model of the transportation system. A Cartesian coordinate (x and z axes) was established at its central position. Since the particle was generally transported in the middle part, where x = -25 to 25 mm in this study, the distributions of the sound pressure on the x-z plane and the x-axis acoustic radiation force in this part were observed. Fig. 6(b) illustrates the structure-acoustic coupling model. The 3 mm thick vibrating plate and the 3mm thick reflector were mounted at a distance of 13 mm, equal to 1.5 times the z-axis wavelength in air. Two vibrational transducers (whose vibration amplitudes were set to 1 μm) were placed 15 mm distant from the free ends. The entire system was surrounded with a 500 mm diameter air zone, which represented an absorbing boundary. To obtain high accuracy and satisfactorily high computing efficiency, the mesh size of the part between the vibrating plate and the reflector [see 'air (inner part)' in Fig. 6(b)] was set

to 0.5 mm and that of the other part [see 'air (outer part)'] was 10 mm. After obtaining the value of the sound pressure, the *x*-axis acoustic radiation force was derived as discussed in the literature [20,31,32] as:

$$F_x = V_{pat} \cdot \frac{3\left(\rho_{pat} - \rho_{air}\right)}{2\rho_{pat} + \rho_{air}} \cdot \frac{\partial E_K}{\partial x} - V_{pat}\left(1-\gamma\right) \cdot \frac{\partial E_p}{\partial x}. \tag{12}$$

Here, V_{pat} is the particle volume, ρ_{air} and ρ_{pat} are respectively the densities of the air and the particle, γ is the ratio of the compressibility of the particle to that of air, and E_K and E_p represent the kinetic energy and the potential energy [20,32] where:

$$E_k = \frac{1}{2}\rho_{air}u^2 \tag{13}$$

and

$$E_p = \frac{p^2}{2\rho_{air}c^2}, \tag{14}$$

respectively. Here, u denotes the vibration velocity of a point in air and is equal to $j/(2\pi f_s \cdot \rho_{air}) \cdot \mathrm{grad}(p)$, where p is the sound pressure at this point and c (= 340 m/s) represents the sound speed in air.

Fig. 7(a) illustrates that the flexural wave has 1.5 wavelengths in the *x* range from -23.5 to 23.5 mm. Fig. 7(b) shows the sound pressure distribution. The wavelength in air is 31.3 mm along the *x* axis, the same as the value for the flexural wave on the plate. Fig. 7(c) shows how the *x*-axis acoustic radiation force was distributed between the vibrating plate and the reflecting plate. It can be seen that in a lattice surrounded with nodal lines, the direction of the acoustic radiation force in the left-

hand part can be contrasted with that in the right-hand part; this infers that particles can be levitated at the central line of the lattice [20]. Previous studies, [3,20,32], have rarely focused on the acoustic radiation force in the *x* axis, so how the *x*-axis acoustic radiation force depends on the SW component is explored, by fitting to the simulation results. It can be seen from Fig. 8 that the *x*-axis acoustic radiation force is proportional to the square of the SW component. On the other hand, it has been reported that the *x*-axis acoustic radiation force induced by the TWs is similar to that for the SWs, proportional to the square of the TW component [33–35]. Thus, when the SWRs are sufficiently small (see Eq. 11), the TW, whose acoustic radiation force is higher than that for the SW, causes the particle to fly in the sound field; this is a qualitative explanation for the continuous mode of the transportation system.

IV. Experimental verification

Fig. 9(a) shows a photograph of the experimental setup, whose configuration is approximately the same as that shown in Fig. 1. The transportation system was driven using a power source made in our laboratories [36,37]. As shown in Fig. 9(b), the vibration velocity on the vibrating plate was obtained by using a scanning Laser Doppler Vibrometer (type PSV500, Polytec). The phase between the vibration velocity of each point and that of a fixed point was obtained using an oscilloscope (type 2024C, Tektronix). Here, the vibration velocity of the fixed point was measured with a single-point

Laser Doppler Vibrometer (type OFV-303, Polytec). During the measurement of the SWRs, the working frequency and the driving voltages on the two transducers were set to 32.875 kHz and 35 V, respectively. Here, the working frequency used was slightly smaller than the series frequency (measured with the impedance analyzer, type 4294A, Agilent) because the vibrating plate was in connection to the transducers [26,38].

First, as an illustration, the SWR of the 310 mm long vibrating plate was explored, when the phase shift was 60°. A TW was observed on the middle part of the vibrating plate [26], corresponding to the range of -130 – 135 mm; while SWs were to be found on the bilateral parts. As shown in Fig. 10(a), the maximum and minimum amplitudes of the vibration velocities were 99.8 and 42.1 mm/s on the middle part, so the SWR was 2.4. Additionally, as shown in Fig. 10(b), the phase difference periodically decreased from 180° to -180° for 9 times in the range of -130 – 135 mm. Therefore, the wavelength is approximately 29.4 mm, closed to the simulated result (30.1 mm).

Next, the SWRs were investigated, as functions of both the vibrating plate length and the phase shift. Fig. 11(a) demonstrates that, when the spatial phase difference and the phase shift satisfy Eq. 11, the SWRs were in the range of 2.6 – 6.1. As predicted, the transportation system works in the continuous mode [see Fig. 11(b)]. In addition, the SWRs have values in the region of several hundred, at l = 300 and 315 mm, while the theoretical values are infinite here; this is probably caused by the discrepancy in the admittance characteristics of the two transducers [27,38]. However, the particle

is not then transportable, as a consequence of the high SWR values. It should be noted that in this study, the vibrating plates having lengths in the range 285 – 315 mm were prepared, with the aim of clarifying how the vibrating plate length affects the transportation performance, within a distance of one wavelength (30.1 mm). When used in practical applications, the length can be selected based on the dependence of the SWR on the length itself, as well as any space constraints from the transportation system overall.

V. Conclusion

In this study, the way in which the SWR and the acoustic radiation force depend on the vibrating plate length and the phase shift are seen, and used to clarify the conditions for generating the continuous mode of the dual transducer type transportation system. When the sum or difference of the spatial phase and the phase shift between the two transducers are $180°\times(1+2n)$ (except where the spatial difference equals $180°\cdot m$ (where m stands for an integer), the SWRs approach unity. Thus, the TW-induced acoustic radiation force pushes the particle so that it can fly through the sound field. These results then clarify the conditions for generating the continuous mode and the work described has shown an excellent approach for the practical design of a dual transducer type ultrasonic levitation-based transportation system. In the future, the work will be extended to construct models to analyze the dynamic properties of the levitated particles and to conduct structural optimization of the

transportation system, to improve its performance.

Acknowledgements

This work was supported by Self-Planned Task (No. SKLRS202003B) of State Key Laboratory of Robotics and System, Harbin Institute of Technology. Grattan K T V and Sun T appreciate the support from the Royal Academy of Engineering.

References

[1] Brandt E H. 2001 Suspended by sound *Nature* **413** 474

[2] Cox L, Croxford A, Drinkwater B W and Marzo A 2018 Acoustic lock: Position and orientation trapping of non-spherical sub-wavelength particles in mid-air using a single-axis acoustic levitator *Appl. Phys. Lett.* **113** 054101

[3] Andrade M A B, Perez N and Adamowski J C 2018 Review of progress in acoustic levitation *Brazilian J. Phys.* **48** 190–213

[4] Ueha S, Hashimoto Y and Koike Y 2000 Non-contact transportation using near-field acoustic levitation *Ultrasonics* **38** 26–32

[5] Dong H-J, Jia L, Guan Y and Zhao J 2017 Experiments and simulations of the standing wave acoustic field produced by two transducers mounted in contraposition *Proc. 2017 Inter. Congr. Ultrasonics* doi: 10.1121/2.0000693.

[6] Zhao S and Wallaschek J 2011 A standing wave acoustic levitation system for large planar objects *Arch. Appl. Mech.* **81** 123–39

[7] Dong H-J, Sui M, Mao C, Mu G and Zhao J 2017 Experiments on the relationship between the structural parameters of contraposition transducers and the acoustic levitation transportation trajectory *Proc. 2017 Inter. Congr. Ultrasonics* doi: 10.1121/2.0001250.

[8] Masuda K, Koyama D and Matsukawa M 2018 Noncontact transportation of planar object in an ultrasound waveguide *IEEE Trans. Ultrason. Ferroelectr. Freq. Control* **65** 2160–6

[9] Xie W J, Cao C D, Lv Y J, Hong Z Y and Wei B 2006 Acoustic method for levitation of small living animals *Appl. Phys. Lett.* **89** 214102

[10] Hashimoto Y, Koike Y and Ueha S 1998 Transporting objects without contact using flexural traveling waves *J. Acoust. Soc. Am.* **103** 3230–3

[11] Ito Y, Koyama D and Nakamura K 2010 High-speed noncontact ultrasonic transport of small objects using acoustic traveling wave field *Acoust. Sci. Techno.* **31** 420–2

[12] Ding M, Koyama D and Nakamura K 2012 Noncontact ultrasonic transport of liquid using a flexural vibration plate *Appl. Phys. Express* **5** 097301

[13] Ueha S, Tomikawa Y, Kurosawa M and Nakamura K 1993 *Ultrasonic Motors—Theory and Applications* (New York, USA: Oxford Univ. Press) pp 148–52

[14] Hashimoto Y, Koike Y and Ueha S 1997 Noncontact suspending and transporting planar objects

by using acoustic levitation *IEEJ Trans. Ind. Appl.* **117** 1406–7

[15] Matsuo E, Koike Y, Nakamura K, Ueha S and Hashimoto Y 2000 Holding characteristics of planar objects suspended by near-field acoustic levitation *Ultrasonics* **38** 60–3

[16] Foresti D, Nabavi M, Klingauf M, Ferrari A and Poulikakos D 2013 Acoustophoretic contactless transport and handling of matter in air *Proc. Natl. Acad. Sci.* **110** 12549–54

[17] Ochiai Y, Hoshi T and Rekimoto J 2014 Three-dimensional mid-air acoustic manipulation by ultrasonic phased arrays *PloS one* **9** e102525

[18] Ochiai Y, Hoshi T and Rekimoto J 2014 Pixie dust: graphics generated by levitated and animated objects in computational acoustic-potential field *ACM Trans. Graphics* **33** 1–13

[19] Hoshi T, Ochiai Y and Rekimoto J 2014 Three-dimensional noncontact manipulation by opposite ultrasonic phased arrays *Jpn. J. Appl. Phys.* **53** 07KE07

[20] Koyama D and Nakamura K 2010 Noncontact ultrasonic transportation of small objects over a long distance in air using a bending vibrator and a reflector *IEEE Trans. Ultrason. Ferroelectr. Freq. Control* **57** 1152–9

[21] Koyama D and Nakamura K 2010 Noncontact ultrasonic transportation of small objects in a circular trajectory in air by flexural vibration of a circular disc *IEEE Trans. Ultrason. Ferroelectr. Freq. Control* **57** 1434–42

[22] Hu J, Nakamura K and Ueha S 2003 Stability analysis of an acoustically levitated disk *IEEE*

Trans. Ultrason. Ferroelectr. Freq. Control **50** 117–27

[23] Osawa K and Nakamura K 2019 High speed non-contact transport of small object in air through ultrasonic traveling field excited with parallel vibration plates *IEEE 2019 Inter. Ultrason. Symp.* doi: 10.1109/ULTSYM.2019.8925797.

[24] Li X, Sun Y, Chen C and Zhao C 2010 Oscillation propagating in non-contact linear piezoelectric ultrasonic transporting system—from solid to fluid media *IEEE Trans. Ultrason. Ferroelectr. Freq. Control* **57** 951–6

[25] Wu J, Mizuno Y and Nakamura K 2020 Piezoelectric motor utilizing an alumina/PZT transducer *IEEE Trans. Ind. Electron.* 67 6762–72

[26] Wu J, Mizuno Y and Nakamura K 2018 Polymer-based ultrasonic motors utilizing high-order vibration modes *IEEE/ASME Trans. Mechatronics* **23** 788–99

[27] Kurosawa M and Ueha S 1989 High speed ultrasonic linear motor with high transmission efficiency *Ultrasonics* **27** 39–44

[28] Graff K F 1991 *Wave Motion in Elastic Solids* (New York, USA: Dover) pp. 180–91

[29] Ide T, Friend J R, Nakamura K and Ueha S, A low-profile design for the noncontact ultrasonically levitated stage *Jpn. J. Appl. Phys.* **44** 4662–5

[30] Aono K, Aoyagi M, Kajiwara H, Tamura H and Takano T 2019 Increase of holding force in near-field acoustic levitation of tabular object inserted between opposing vibration sources *Jpn. J. Appl.*

Phys. **58** SGGD11

[31] Bruus H 2012 Acoustofluidics 7: The acoustic radiation force on small particles *Lab Chip* **12** 1014–21

[32] Baer S, Andrade M A B, Esen C, Adamowski J C, Schweiger G and Ostendorf A 2011 Analysis of the particle stability in a new designed ultrasonic levitation device *Rev. Sci. Instruct.* **82** 105111

[33] King L V 1934 On the acoustic radiation pressure on spheres *Proc. Royal Soc. A* doi: 10.1098/rspa.1934.0215.

[34] Settnes M and Bruus H 2012 Forces acting on a small particle in an acoustical field in a viscous fluid *Phys. Rev. E* **85** 016327

[35] Doinikov A A 1997 Acoustic radiation force on a spherical particle in a viscous heat-conducting fluid. II. Force on a rigid sphere *J. Acoust. Soc. Am.* **101** 722–30

[36] Dong H-J, Wu J, Zhang G-Y and Wu H-F 2012 An improved phase-locked method for automatic resonance frequency tracing based on static capacitance broadband compensation for a high-power ultrasonic transducer *IEEE Trans. Ultrason. Ferroelectr. Freq. Control* **59** 205–10

[37] Dong H-J, Wu J, Zhang H and Zhang G-Y 2011 Design and development of a multi-hole broadband-based ultrasonic transducer *Ultrason. Sonochemist.* **18** 562–6

[38] Nakamura K 2020 Evaluation methods for materials for power ultrasonic applications *Jpn. J. Appl. Phys.* **59** SK0801

Table

Table I Equivalent circuit parameters of the Langevin transducers

	$1^{\#}$	$2^{\#}$
Serial frequency, f_s (kHz)	33.364	33.533
Parallel frequency, f_p (kHz)	33.824	34.188
Mechanical quality factor, Q	599	928
Motional admittance, Y_m (mS)	16.862	36.724
Motional resistance, R_m (Ω)	59.305	27.230
Motional inductance, L_m (H)	0.169	0.120
Motional capacitance, C_m (pF)	134.445	188.067
Clamped capacitance, C_d (nF)	4.912	4.777

Figures and captions

Fig. 1 Conceptual view of the dual transducers-type ultrasonic levitation-based transportation system. Here, $U_0\cos(\omega t)$ and $U_0\cos(\omega t + \theta)$, where U_0, ω, and θ are respectively the amplitude, the angular frequency, and the phase of the applied voltage.

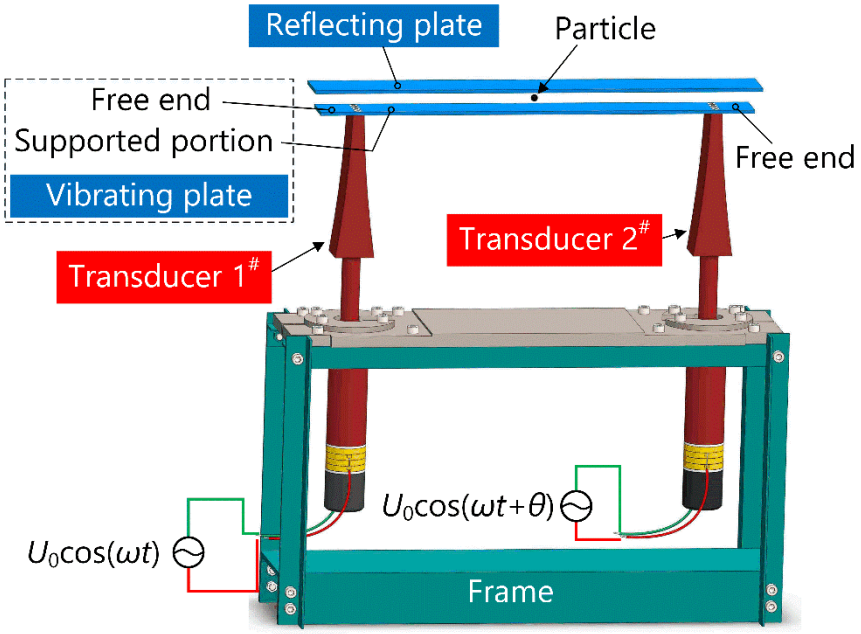

Fig. 2 Configuration and dimensions of the Langevin transducers.

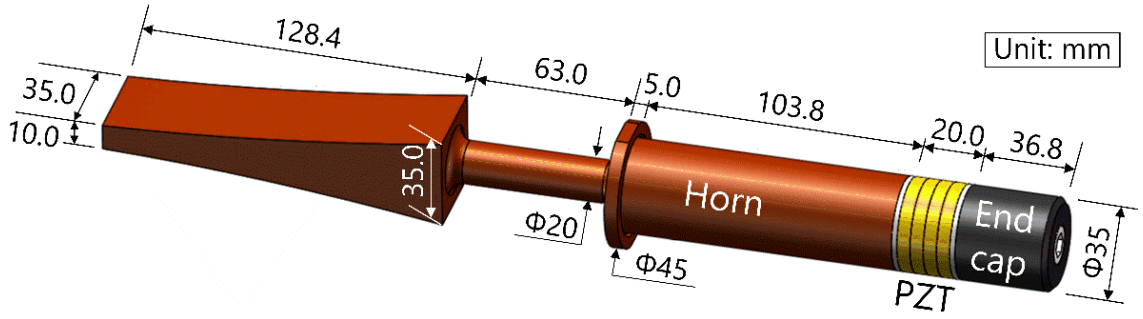

Fig. 3 Equivalent transducer array model. (a) Distribution of the nodes, (b) the equivalent transducer array (where deep-gray transducers are actual ones, whereas light-gray transducers are imaginary ones), and (c) the phase corresponding to each transducer.

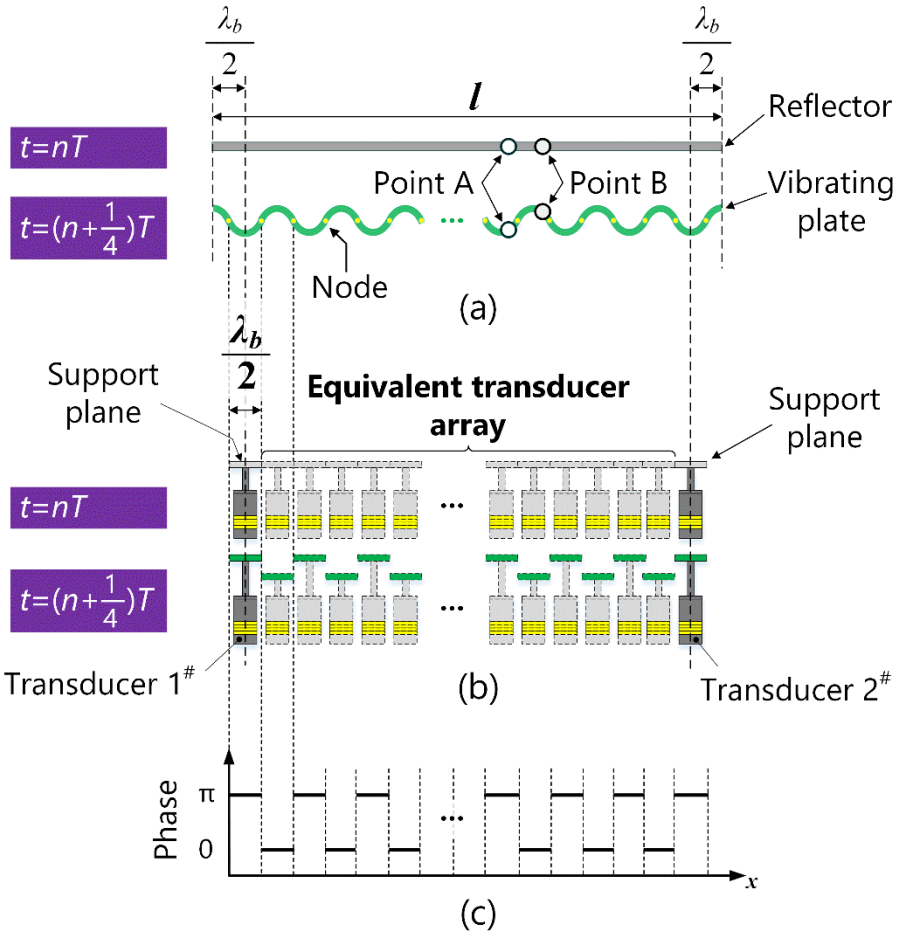

Fig. 4 SWRs as functions of the phase shift at l = 310 mm.

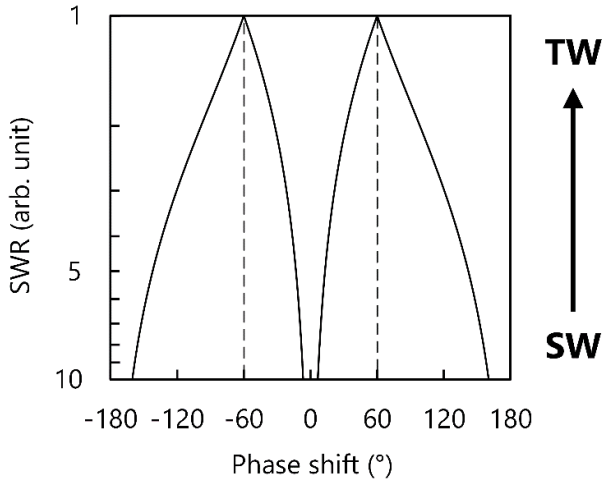

Fig. 5 Variation in SWRs against the vibrating plate length and the phase shift.

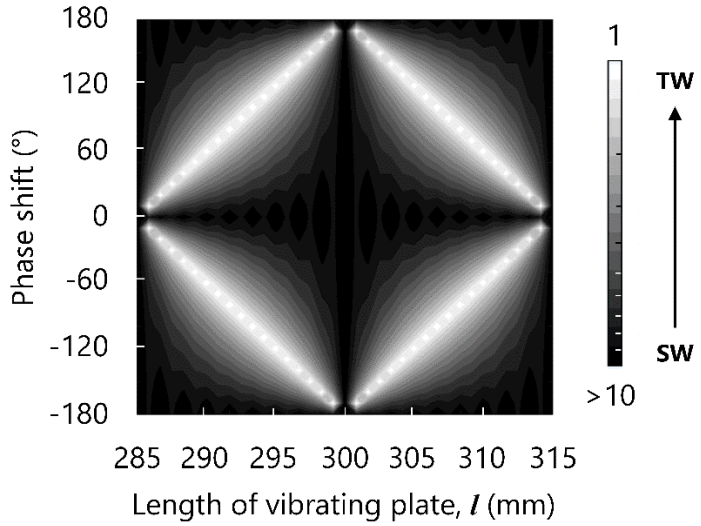

Fig. 6 Simplified model for analyzing the sound field and the *x*-axis acoustic radiation force. (a) Configuration and (b) FEA model.

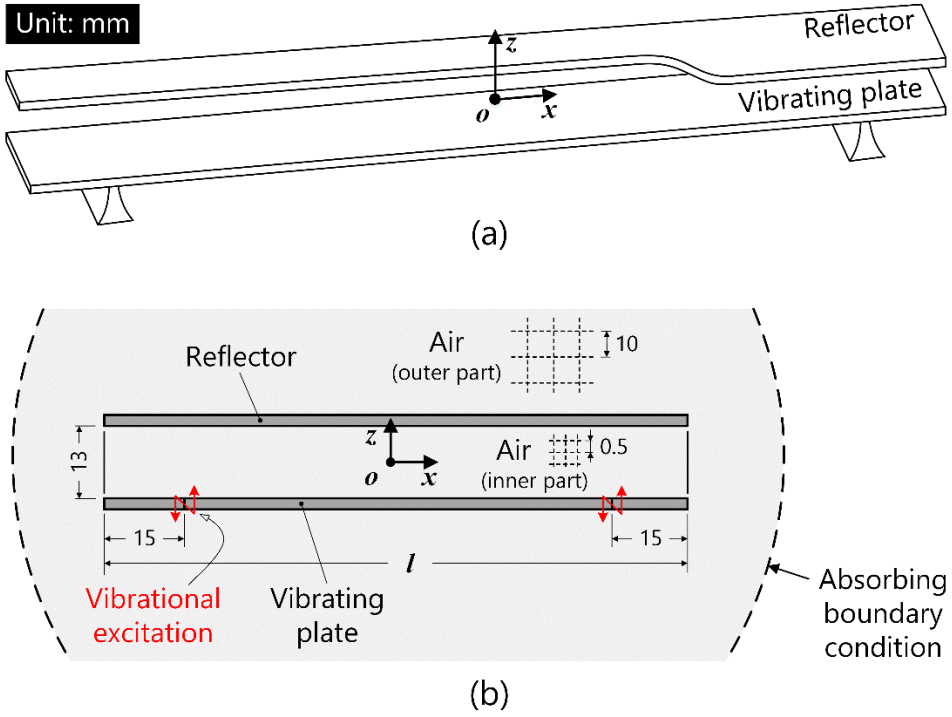

Fig. 7 (a) Vibration displacement on the vibrating plate, (b) sound pressure distribution, and (c) *x*-axis acoustic radiation force. The values shown in (b) and (c) are normalized values.

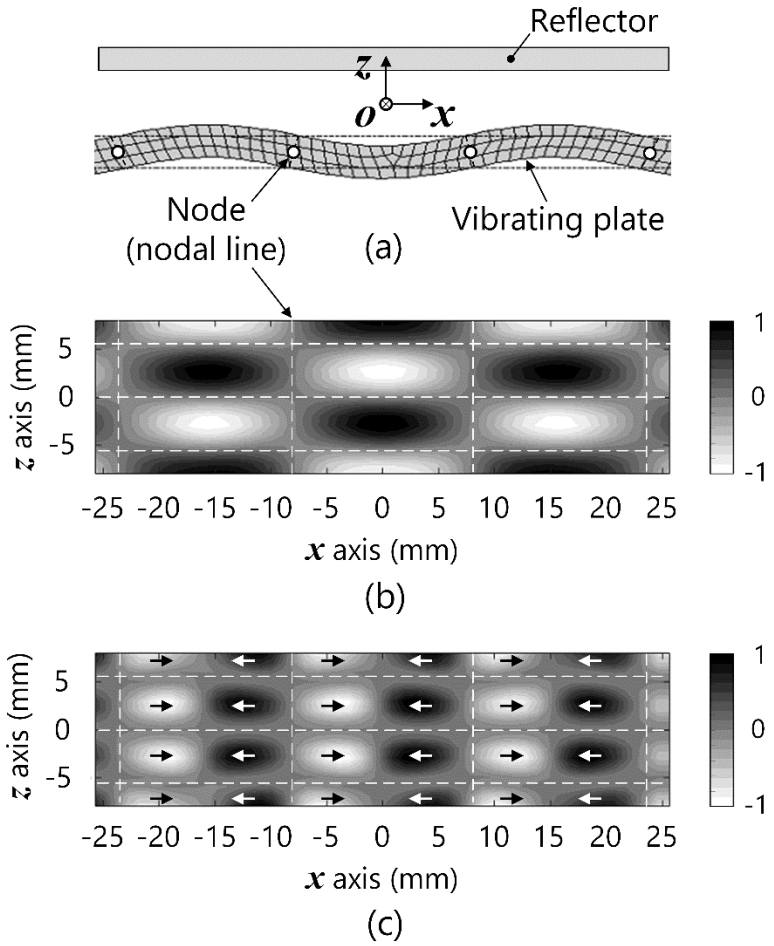

Fig. 8 Normalized values of the *x*-axis acoustic radiation force versus the amplitude of the standing wave component.

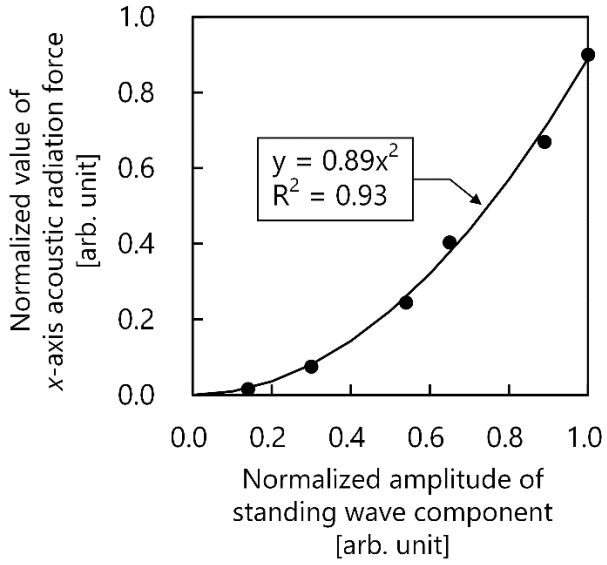

Fig. 9 Experimental setup. (a) Transportation system and (b) measurement of the vibration velocity.

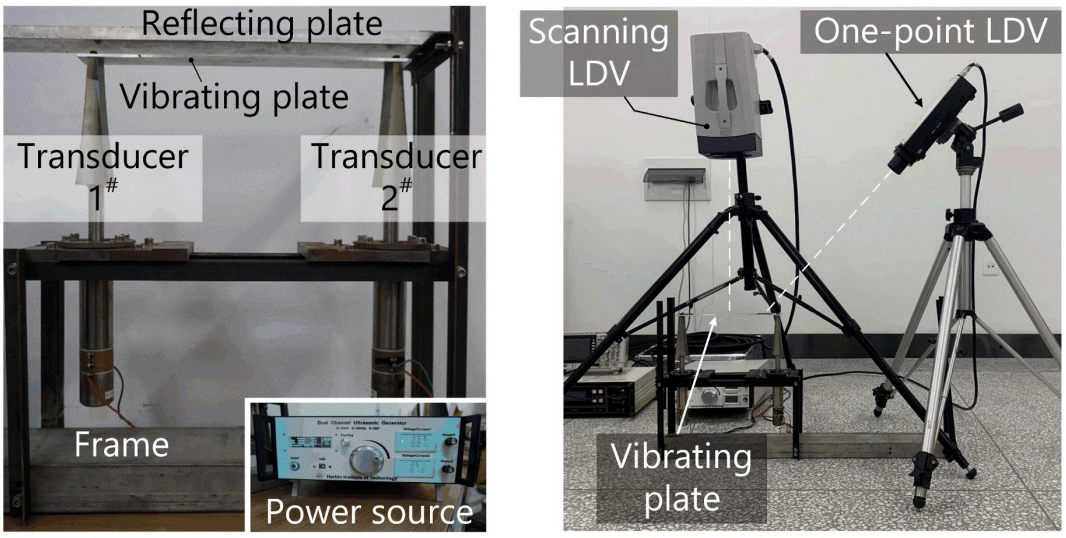

Fig. 10 Distributions of (a) the vibration velocity amplitude and (b) the phase difference inside two wavelengths along on the 310 mm long vibrating plate when the dual transducers being excited at the phase shift of 60°. These values were measured by the authors using the vibrometer (type PSV-500, Polytech).

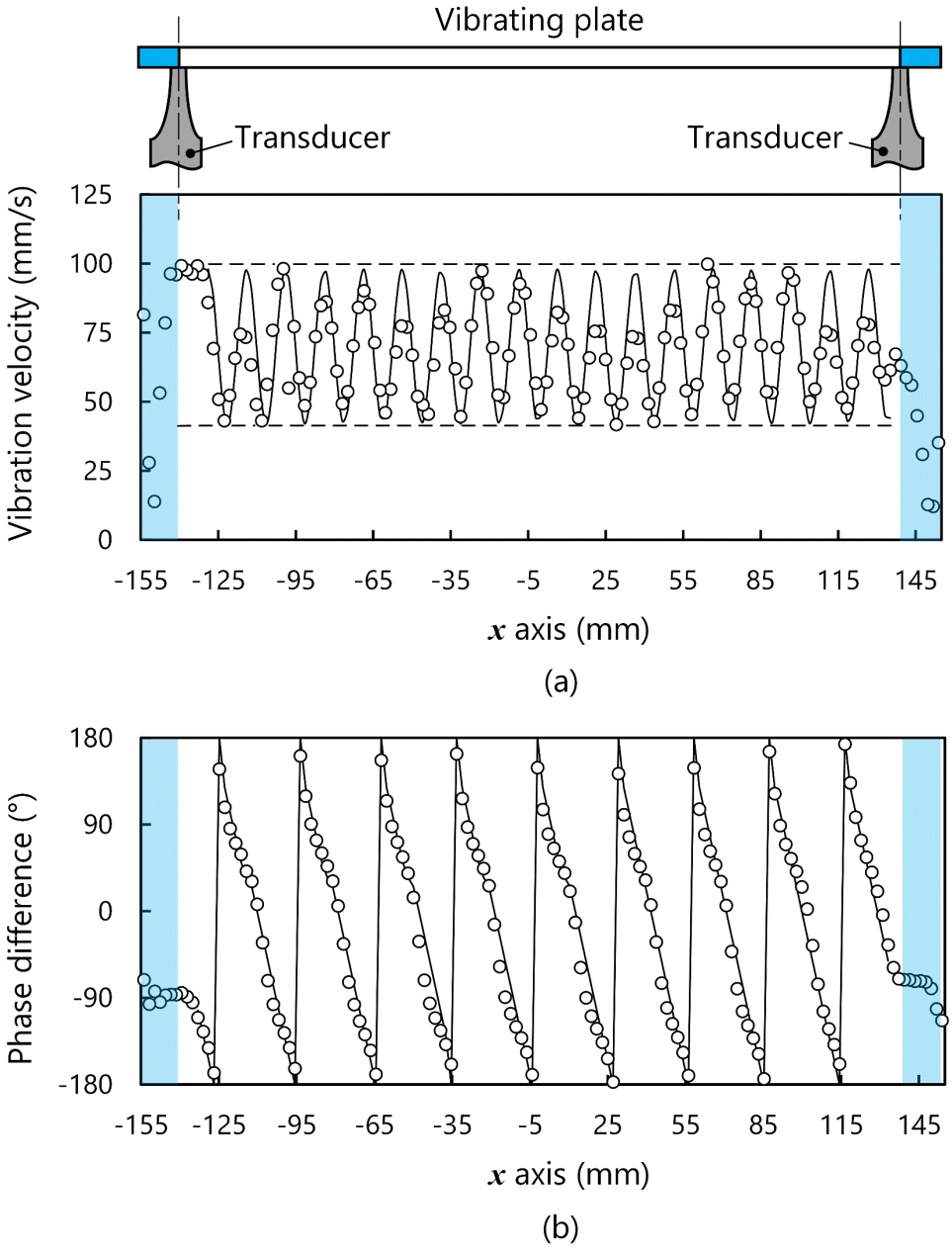

Fig. 11 (a) Measured SWRs (the numbers indicated close-to/surrounded-with the dots) and (b) transport states versus the vibrating plate's length and the phase shift. In (b), the dots indicate that the particle are continuously transported while the cross marks mean the particles are not transportable.